Inclusion of compensator-induced scatter and beam filtration in pencil beam dose calculations

F. C. P. du Plessis[a)] and C. A. Willemse
Medical Physics Department, Faculty of Health Sciences, University of the Free State, P.O. Box 339, Bloemfontein, 9300 South Africa

(Received 29 March 2006; revised 13 June 2006; accepted for publication 14 June 2006; published 24 July 2006)

Compensators can be used as beam intensity modulation devices for intensity-modulated radiation therapy applications. In contrast with multileaf collimators, compensators introduce scatter and beam hardening into the therapeutic x-ray beam. The degree of scatter and beam filtering depends on the compensator material and beam energy. Pencil beam dose calculation models can be used to derive the shape of the compensator. In this study a novel way of incorporating the effect of compensator-induced scatter and beam filtration is presented. The study was conducted using 6, 8, and 15 MV polyenergetic pencil beams (PBs). The compensator materials that were studied included wax, brass, copper, and lead. The perturbation effects of the compensators on the PB dose profiles were built in the PB dose profiles and tested for regular fields containing a step compensator and benchmarked against DOSXYZnrc Monte Carlo calculated dose profiles. These effects include compensator beam filtration and Compton-scattered photons generated in the compensator materials that influence the resulting PB dose profiles. These data were obtained from DOSXYZnrc simulations. A Gaussian function was used to model off-axis scatter and an exponential function was used to model beam hardening at any radius, r. Dose profiles were calculated under a step compensator using the method that can model beam hardening and off-axis scatter, as well as a conventional method where the PB profiles are not adjusted, but a single effective attenuation coefficient is used instead to best match the dose profiles. Both sets of data were compared to the DOSXYZnrc data. Depth and profile dose data for 10×10 cm^2 and 20×20 cm^2 fields indicated that at 2 cm depth in water the method that takes compensator scatter into account agrees more closely with the DOSXYZnrc data compared to the data using only an effective attenuation coefficient. Further, it was found that the effective attenuation method can only replicate the DOSXYZnrc data at 10 cm depth where it was chosen to do so. At shallower depths the effective attenuation method overestimates the dose and beyond 10 cm depth it causes an underestimation in the dose. The scatter and beam hardening inclusion method does not exhibit such properties. The exclusion of scatter can lead to dose errors of up to 4 percent with a copper compensator at 5 cm depth for a 10×10 cm^2 field under a thickness of 5 cm at 6 MV. For materials such as lead this discrepancy could be as high as 7 to 8 percent at 6 MV. For larger fields (20×20 cm^2) the effect of in-phantom scatter reduces the differences between the dose profiles calculated with the mentioned methods.
[DOI: 10.1118/1.2219777]

Key words: Pencil beam, compensator, scatter, DOSXYZnrc, EGSnrc, Monte Carlo

I. INTRODUCTION

Pencil beam (PB)-based dose calculation algorithms can be used to calculate dose distributions for irregular-shaped fields, e.g., partially blocked photon fields or multileaf collimator (MLC)-shaped fields in intensity modulated radiation therapy (IMRT). Intensity modulation can be achieved using MLC, dynamic jaws,[1] wedges, masks,[2] or compensators.[3–6] IMRT is usually accomplished by delivering sets of beam segments at different gantry angles. These segments are derived by analysis of the optimized fluence map for each gantry angle using a leaf sequencer algorithm. These fluence maps in turn are derived from an optimization process that assigns weights to beamlets. The net result is that the total dose contribution of these beamlets will be the optimal dose for the IMRT plan. The map of beamlet weights will correspond to the fluence map of the field. Compensators can be used to approximate this fluence map by appropriate attenuation of the individual beamlets making up the original open beam fluence.

A MLC can shield a beam resulting in low beam transmission.[7,8] Beamlet weighting can be viewed as the fraction of the time it contributes to the total dose for the beam compared to the total treatment time. However, transmission corrections are crucial for relative dose calculations.[9] In the case of compensators, dose modulation is achieved by attenuating the energy fluence so that the dose contribution is effectively weighted. Compensators would introduce spectral changes in the heterogeneous photon beam that will alter its in-phantom scatter and beam penetration

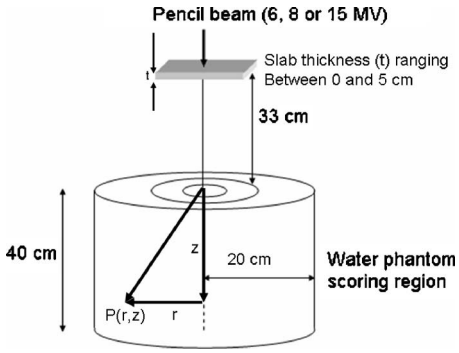

FIG. 1. Dose recording geometry setup in DOSRZnrc to obtain the 3D dose of a scattered and filtered pencil beam after traversing the shown compensator slab material. The materials used were wax, copper, brass, and lead for beam energies of 6, 8, and 15 MeV, respectively. The cylindrical water phantom is 40 cm thick and has a diameter of 40 cm.

properties. It also produces a compensator-scatter background[10] through coherent scatter events at megavoltage energies.

Beamlets can be modeled using Monte Carlo (MC) methods[11] or pencil beams[12–17] or a combination of both methods in optimized treatment planning.[18] When 3D PB dose calculations are performed the energy fluence at the point of entry in the patient model must be known. This, in turn, depends on the number of photons which can scatter from the jaws, beam modulators, flattening filter,[19–22] and collimators.[23] Some authors have treated the problem of scatter and spectral changes in the fluence by analytical models[19–21] that correct for the primary and scatter fractions of the energy fluence emanating from the flattening filter, collimator, and a modulator, e.g., a wedge or compensator. Others have used a Compton first-scatter-based method to calculate the scatter fluence from a beam-modifying absorber,[24] approximations for second-order scatter,[25] and semiempirical methods that include sector integration.[26–28] Weber *et al.*[29] applied an analytical method[19] in conjunction with a k_μ matrix to take off-axis spectral changes of the polyenergetic photon beam into account. In this study a novel way of incorporating the effect of compensator-induced scatter and beam filtration is presented that differs from photon scatter kernel-based methods. The study was conducted using 6, 8, and 15 MV polyenergetic pencil beams (PBs). The compensator materials that were studied included wax, aluminum, brass, copper, and lead. The perturbation effects of the compensator materials on the PB dose profiles were included in PB dose calculations for the case of a regular field containing a step-shaped attenuator. The results were compared with Monte Carlo-based DOSXYZnrc (Ref. 30) dose calculations in a water phantom for the corresponding situation for two field sizes.

II. METHODS

Figure 1 shows the simulation geometry used. The EGSnrc (Ref. 31)-based DOSRZnrc MC code was used to simulate sets of polyenergetic PBs for energies of 6, 8, and 15 MV. Three-dimensional (3D) dose distributions were recorded in a cylindrical water phantom after photon PBs were transported through varying thicknesses (t=0, 1.0, 2.0, 3.0, and 5.0 cm) of compensator material consisting either of pure wax, aluminum, brass, copper, or lead. The 3D dose distribution scored in the cylindrical phantom for a single PB with no attenuator will be referred to as an open PB. The water phantom had a height of 40 cm and a radius of 20.0 cm, which was further subdivided into 50 annuli each with a width ((Δr) of 0.4 cm. In the z direction (depth in phantom) the height of the phantom was subdivided into 20 slabs of 0.20 cm thickness, starting at the surface, followed by 36 slabs of 1.0 cm thickness. The distance between the compensator material and the water surface was 33 cm.

The DOSRZnrc code was chosen since pencil beams display cylindrical spatial symmetry in homogeneous media. The energy spectra for the PB models were based on the Philips SL74/14N, SL75-5 and SL-25 linac series and were obtained previously by the authors[32] using the EGS4 (Ref. 33)-based BEAM (Ref. 34) MC code to simulate radiation transport through these accelerator models. Output beam data were scored in phase-space files (PSF) and were analyzed with the BEAMDP (Ref. 35) code. Each PSF contained the primary and scattered photons from the radiation head from which these energy spectra were derived.

The direction of incidence of the PB was parallel to the Z direction with the point of entry on the origin of the phantom. To study the perturbing effect of a compensator material with thickness (t) located in the path of the PB, 200 million histories were simulated for each thickness. The energy cutoffs for electron (ECUT) and photon (PCUT) transport were set at 0.700 and 0.010 MeV, respectively, below which the energy was deposited locally and the transport of the particle was terminated. Spin effects were also included in the simulations. Each 3D dose distribution of the perturbed PBs was normalized to its own dose maximum on the z axis. The depth in the water phantom is denoted by z, and the compensator thickness by t.

To study the perturbation effect of the compensator material, a mathematical model was constructed based on the open PB by addition of two components to account for relative beam filtration and off-axis scatter. By applying this model the effect of the compensator material can be added to the open PB.

In order to fit the mathematical model to the PB dose profiles, the effective radius of each annulus had to be determined. Pencil beams can be determined from basic data.[36] For the purpose of this study, PBs were generated using the cylindrical geometry of the DOSRZnrc MC code since it allows one to achieve variance reduction by scoring the particles in annuli rather than in the much smaller rectilinear voxels in Cartesian space. It also allows the PB dose profiles to be described accurately with the analytical equation[20,23]

$$P_o(r,z) = \frac{A(z)\exp(-B(z)r)}{r} + \frac{C(z)\exp(-D(z)r)}{r}, \qquad (1)$$

where $A(z)$ to $D(z)$ are the fitting parameters at each depth (z) in the phantom. The second term can be regarded as the

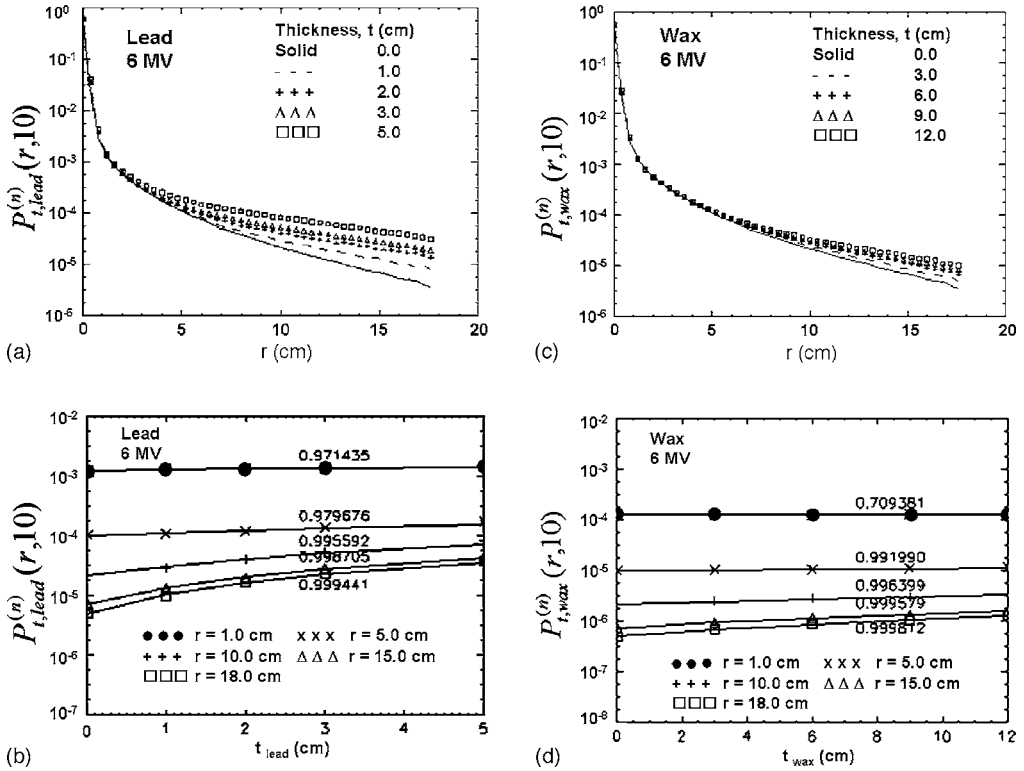

FIG. 2. (a) A set of normalized 6 MV pencil beam dose profiles in the DOSRZnrc water phantom after traversing different thicknesses of lead (0, 1, 2, 3, and 5 cm) and wax [shown in (c)]. Panels (b) and (d) show the relative dose $p^{(n)}_{t,\mathrm{med}}$ vs absorber thickness (t) at radii of 1, 5, 10, 15, and 18 cm.

scatter component and the first term is assumed to be the primary energy imparted, although the degree of precision might not be high.[23]

Due to the finite width of the annuli and the large radial dose gradient near the PB axis, the effective radius of each annulus was determined by using the formalism of Wang *et al.*[37] They used the formula

$$r_n = \left[(n+0.5) + \frac{1}{12(n+0.5)} \right] \Delta r, \tag{2}$$

where n is the annulus index with values $n=(0,1,2,\ldots,n)$ and Δr is the physical width of the annulus. The diameter of the incident PB coincided with the diameter of the central annulus since this leads to the best accuracy in the PB parametrization [Eq. (1)] when using the radius values, r_i, calculated with Eq. (2). The effect of Eq. (2) on the calculated radii is largest for $n=0$ (the first annulus), e.g., the radius r_0 would be $\frac{2}{3}\Delta r$ instead of $\frac{1}{2}\Delta r$ defined by the geometric center of the first annulus. For the outer annuli where n becomes large the effective radius r_n would approach the value $r_n \rightarrow (n+0.5)\Delta r$.

The model was validated by comparing dose profiles of the modified open PB with MC derived profiles for PBs transported through the compensator material. Also, a comparison was made between fractional depth-dose curves calculated with the open PB, the modified open PB (to include scatter and beam filtering), and real attenuated PBs (obtained from MC simulations by transporting the PB through the compensator material). In a further test step-shaped compensators were used in a series of DOSXYZnrc MC simulations to determine the dose in water at 2, 5, 10, and 15 cm depth using field sizes between 10×10 cm^2 and 20×20 cm^2 for the three beam energies and compensator materials used in this study. The relative dose profiles were then compared with profiles for the PB calculations under the same compensator shape.

III. RESULTS AND DISCUSSION

A. Relative pencil beam dose profiles vs compensator slab thickness

Figures 2(a) and 2(c) show two sets of normalized PB profiles for 6 MV. Each normalized PB traversed different thicknesses of the compensator material indicated as lead and wax. It will hereafter be referred to as the relative dose and indicated as $P^{(n)}_{t,\mathrm{med}}(r,z)$, with t and med indicating the thickness and material (medium) of the absorber and (n) indicating that it is normalized. The unnormalized dose will be indicated as $P_{t,\mathrm{med}}$ and is related to $P^{(n)}_{t,\mathrm{med}}$ through: $P^{(n)}_{t,\mathrm{med}} = P_{t,\mathrm{med}}/(P_{t,\mathrm{med}})_{\max}$ where $(P_{t,\mathrm{med}})_{\max}$ indicates the maximum dose on the PB axis.

The profiles in Figs. 2(a) and 2(c) were scored at a depth of 10 cm in the water phantom model. Similar data were found for 8 and 15 MV beam energies albeit not shown here. At any given off-axis distance the value of the normalized PB dose profiles increases as the slab thickness (t) increases. This can be attributed to increasing numbers of photons being scattered away from the PB axis with increase in thick-

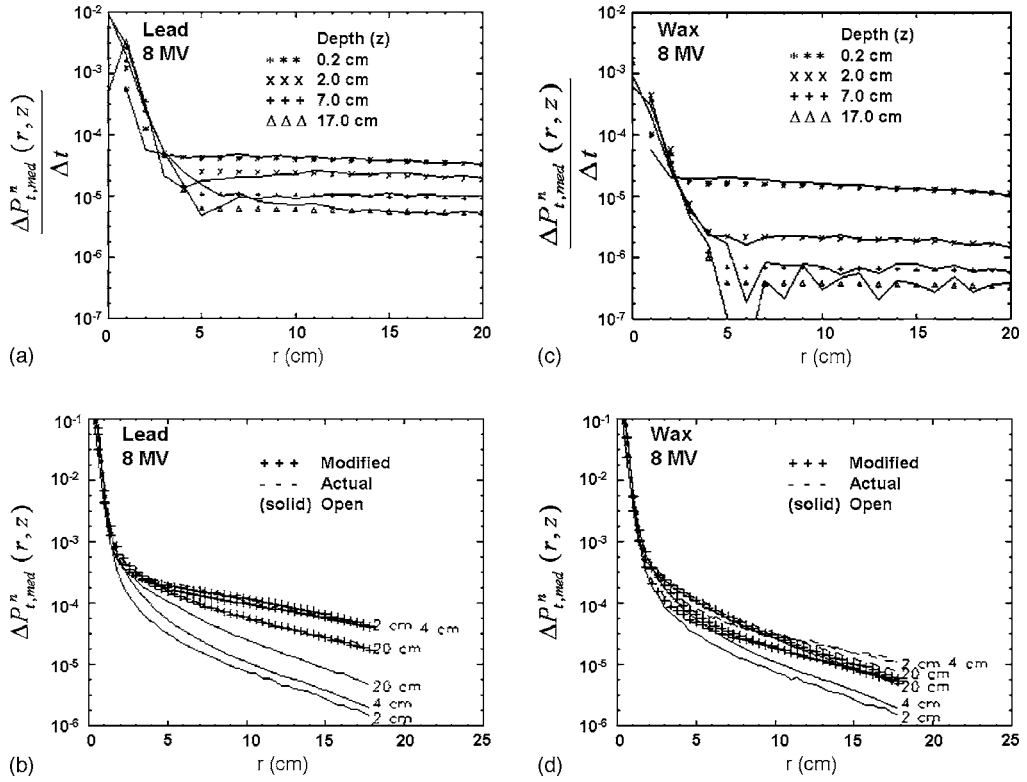

FIG. 3. (a) and (c) The change in the relative dose per unit absorber thickness ($\Delta P^{(n)}_{t,\mathrm{med}}/\Delta t$) at 8 MV as a function of radial distance from the PB axis. Data shown are for depths of 0.2, 2.0, 7.0, and 17.0 cm in the DOSRZnrc water phantom. A Gaussian function was fitted to the data beyond the transition radius at each depth. A function [Eq. (4)] was also fitted to the data points at each depth between the beam axis and the transition radius. Panels (b) and (d) show the modified open PB profiles at 2, 4, and 20 cm depth are compared to the actual profiles $p^{(n)}_{t,\mathrm{med}}$.

ness of compensator. At the studied megavoltage photon energies the incoherent (Compton) scatter process would dominate. The number of photons scattered in a given direction will be proportional to the number of target electrons, which in turn will be proportional to the thickness of the compensator. Therefore, at any given off-axis position, the relative dose under the compensator, compared to the open PB, would increase with increasing compensator thickness.

Figures 2(b) and 2(d) show two sets of plots of the PB fractional dose as a function of absorber thickness (t) at radial positions of 1, 5, 10, 15, and 18 cm. The data were fitted with a linear function vs thickness and the correlation of fit (R^2) is shown on each line. Note that on the logarithmic scale the lines appear to be curved.

From these results, in principle, the radial dose profile of an open PB can be adjusted to account for the effect of its transmission through a slab of compensating material of known thickness. The linear relationship between relative scattered dose vs compensator thickness was found to apply to all energies and materials used in this study, ranging from wax with the lowest density up to lead.

The materials used in this study have an electron density range from low (wax) to high (lead), and all of them showed a linear relationship between relative scatter dose and compensator thickness. Thus, any compensator material falling within this electron density range should exhibit a similar relationship.

Although not studied here, the above trend indicates that for even higher atomic number and electron density compensators like tungsten, this trend should also hold. Beam filtration depends on the absorbers' ability to filter out low energy components from the beam by means of photoelectric absorption or scattering out photons by means of Compton interactions. The number of Compton interactions per unit volume would depend on the electron density of the material. For tungsten the photoelectric cross section is higher than for lead and the number of Compton-scattered photons is also higher per unit volume and thus would enhance the relative dose more at locations away from the CAX compared with that for lead compensators.

B. Relative scatter dose and beam filtration

The combined effect of beam filtration and photon scatter causes an increase in the off-axis PB dose distribution when it passes through a compensating medium. The increase in the dose relative to the open PB profiles is approximately linear in the thickness of the compensator material as shown in Figs. 2(b) and 2(d). From these data the slopes ($\Delta P^{(n)}_{t,\mathrm{med}}/\Delta t$) of the fitting lines ($P^{(n)}_{t,\mathrm{med}}$ vs t) were determined at each depth, z, and radial position, r, of the annular bins used in the water phantom.

Figures 3(a) and 3(c) show some of the slope values (solid lines) for the case of 8 MV. Similar data were also obtained

for 6 and 15 MV beam energies but not shown here. The plots are for four arbitrary chosen depths (z) of 0.2, 2.0, 7.0, and 17 cm, respectively. [Note: In these plots the raw data (left column) are shown connected by straight line segments to improve the visual appearance only. The symbols represent fitted functions that were derived as described hereunder.]

The slopes $\Delta P_t^{(n)}/\Delta t$ indicate the rate of change in the relative dose per unit absorber thickness. For the cases shown $\Delta P_t^{(n)}/\Delta t$ is large near the PB axis, becoming rapidly smaller at a certain transition radius from where it decreases gradually beyond this radius. The transition radius, beyond which the $\Delta P_t^{(n)}/\Delta t$ starts to change more gradually, is of the order of 2 cm near the water phantom surface, but increases to 4 cm at 17 cm depth for 6 MV PB. For the 8 MV case shown and for a 15 MV case (not shown) the corresponding radii are 3 to 5 cm and 3 to 7 cm, respectively. Beyond the transition radius, the enhancement in the PB dose profiles relative to an open PB is considered to be caused by compensator-induced scatter. In this study $\Delta P_t^{(n)}/\Delta t$ values beyond the transition radius were fitted with a Gaussian function [Eq. (3)] for all energies and materials used,

$$\alpha(r,z) = a_1(z)\exp[-a_2(z)r^2]. \tag{3}$$

The radial distance is indicated by r as measured from the PB axis and $a_1(z)$ and $a_2(z)$ are fitting parameters that are functions of depth, energy, and compensator material.

In Figs. 3(a) and 3(c) the Gaussian data fits are shown as symbols and starts just beyond the transition radius.

In the following step $\Delta P_t^{(n)}/\Delta t$ values as obtained from the Gaussian fits were subtracted from the raw $\Delta P_t^{(n)}/\Delta t$ data over the total radius range. The residue $\Delta P_t^{(n)}/\Delta t$ values beyond the transition radius were set to zero. The remaining $\Delta P_t^{(n)}/\Delta t$ residues were fitted by the function represented in Eq. (4),

$$\beta(r,z) = b_1(z)[r - b_2(z)]\exp[-b_3(z)r], \tag{4}$$

where r is the radial distance and $b_1(z)$, $b_2(z)$, and $b_3(z)$ are fitting parameters which are functions of depth, energy, and compensator material.

Equation (3) represents the relative scatter enhancement due to the presence of a compensating medium, and Eq. (4) the dose alteration on the PB axis most probably due to beam filtering and hardening of the open PB. $\Delta P_t^{(n)}/\Delta t$ can be modeled with

$$\frac{\Delta P_t^{(n)}(r,z)}{\Delta t} = \alpha(r,z) + \beta(r,z). \tag{5}$$

To further highlight the concept, Fig. 4 shows the comparative difference, $P_{t,\text{brass}}^{(n)} - P_0^{(n)}$, in the normalized dose profiles relative to an open PB after traversing different thickness of brass absorbers at 8 MV and 10 cm depth in water. The normalized point was taken at the dose maximum of the open PB.

From Fig. 4 it can be observed that the relative dose is highest for the open PB that traversed the 5 cm brass slab. The thicker slab causes more scatter events of the photons

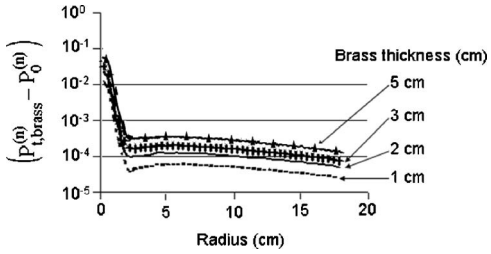

FIG. 4. Dose enhancement on dose profiles at 10 cm depth for normalized pencil beams that traversed different thicknesses of brass slabs relative to an open pencil beam ($P_{t,\text{brass}}^{(n)} - P_0^{(n)}$). The thickness of the brass slabs was 1.0, 2.0, 3.0, and 5.0 cm and the beam energy was 8 MV.

that lead to a relative higher dose at off-axis locations. Near the PB axis, the relative dose enhancement increases abruptly as the off-axis distance reduces. This effect is largest for the 5 cm brass case and can be ascribed to beam filtering or hardening causing a larger discrepancy in the normalized absorbed dose.

C. PB dose scaling using open PB

It is proposed that compensator scatter and beam quality alteration can be accounted for by using the open PB and adjusting its profiles using Eqs. (3) and (4). The linear relation between the relative dose $P_{t,\text{med}}^{(n)}$ and absorber material thickness (t) [shown in Figs. 2(b) and 2(d)] can be used to determine the change in the PB dose profile for a given attenuator thickness (t) based on the 3D dose distribution of an open PB, $P_0^{(n)}$. The intercepts on the ordinate axis ($t=0$) of the fitted lines in Figs. 2(b) and 2(d) are equivalent to the normalized absorbed dose for the open PB. The perturbation to the relative dose due to the presence of an attenuator can be modeled as

$$P_{t,\text{med}}^{(n)}(r,z) = P_0^{(n)}(r,z) + \alpha(r,z)t + \beta(r,z)t \tag{6}$$

where $\alpha(r,z)$ and $\beta(r,z)$ are obtained from Eqs. (3) and (4). $P_{t,\text{med}}^{(n)}(r,z)$ represents the normalized (n) 3D PB dose distribution for an open PB [$P_0^{(n)}(r,z)$] traversing a medium (med) with thickness (t). Since the compensator material lowers the total dose contribution due to photon interaction events, it is assumed as a first approximation that $(P_{t,\text{med}})_{\max} = (P_0)_{\max}\exp(-\mu_{\text{eff}}t)$, with μ_{eff} representing a narrow-beam effective attenuation coefficient. The unnormalized dose will then be given by $P_{t,\text{med}} = P_{t,\text{med}}^{(n)}(P_{t,\text{med}})_{\max}$, and thus

$$P_{t,\text{med}} = P_{t,\text{med}}^{(n)}(P_0)_{\max}\exp[-\mu_{\text{eff}}(z)t], \tag{7}$$

This is an approximation because $(P_0)_{\max}$ and $(P_{t,\text{med}})_{\max}$ do not necessarily occur at the same depth (z).

D. Alteration of fractional depth-dose data due to the presence of a compensator

The dose profile modeling scheme as outlined in Eqs. (3)–(6) was tested and the results are shown in Figs. 3(b) and 3(d). In each graph the solid line indicates the dose profile for the open PB at 2, 4, and 20 cm depth in the DOSXYZnrc (Ref. 38) water phantom. For the corresponding depths the

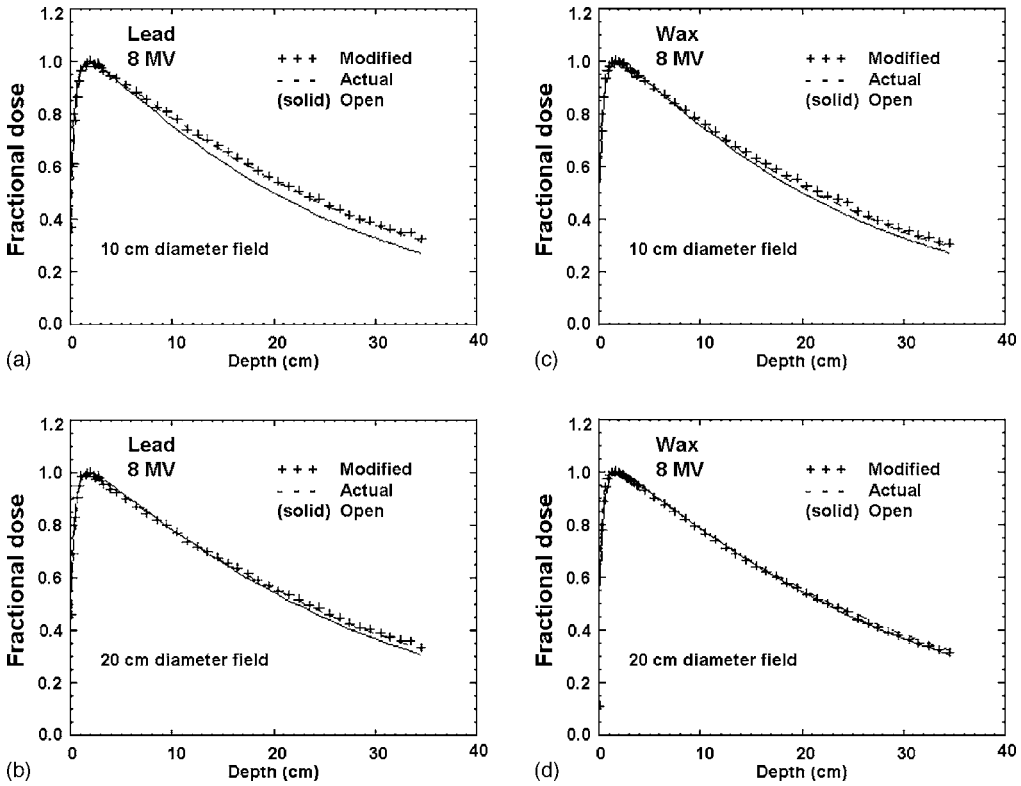

FIG. 5. (a) Fractional depth-dose curves at 8 MV for a 10 cm circle field for lead and wax (b) compensators. The solid line represents the FDD curve derived from the open PB. The broken line represents data derived from simulations of the actual transport of the open PB through 5 cm of lead and 12 cm of wax material. The symbols indicate data calculated from the modified PB data. In panels (b) and (d) similar data are shown for a circle field with a 20 cm diameter.

dose profiles are also shown for the PB after traversing 5 cm of absorber material and are shown as dotted lines. These data were obtained from MC simulations of the actual transport of the open PB through the compensating material. The profiles shown for wax were obtained for 12 cm thickness. The modified open PB dose profiles are shown as "+++" symbols after setting $t=12.0$ cm for wax and 5.0 cm for lead. The agreement between the fully simulated PB data (dotted lines) and the modified open PB data as calculated with Eqs. (3)–(6) shows good agreement especially for the wax material, but shows slight discrepancies for lead. See Ref. 39.

In order to test the effect of these discrepancies fractional depth-dose data (FDD) were derived for nondiverging circular fields with diameters of 10 and 20 cm for the following three cases; in case 1 the open PB only was used to calculate the FDD. In case 2 the FDD was calculated using the modified open PB data for the 8 MV case for wax and lead. In case 3 the FDD was calculated from the actual PB data derived from MC simulations as described above and were used as a benchmark. The results are shown in Figs. 5(a)–5(d).

Depth-dose data were calculated using the cylindrical PB and utilizing the reciprocity theorem, i.e., for a 10 cm circular field the dose in each annulus was summed up to a radius of 5 cm. The sum of the dose values in each annulus would yield the dose on the PB axis. For the wax and lead data at 8 MV the correspondence between the depth doses obtained with the modified open PB and those obtained with the benchmark (actual) PB is within a margin of 1 percent for the two circular fields investigated.

For the other materials and beam energies used in this study the correspondence was within 1 percent between the modified open PB derived and the benchmark FDD curves over both field sizes used.

The 10 cm circular field in Figs. 5(a) and 5(b) shows a deviation of the open PB derived FDD and the real PB derived FDD that is higher for lead compared to wax as a function of depth. It could be ascribed to more effective beam filtering by lead leading to a beam with higher effective energy causing an increase in the penetration power of the beam. This increase for lead can be up to 6 percent at large depths. For the 20 cm circle field the increase in in-phantom scatter compared to the 10 cm circle field reduces the PB filtering effect of lead, i.e., more dose is deposited due to in-phantom scatter on the central axis (CAX), which in turn counters the effects of beam hardening on the CAX. For smaller fields CAX beam hardening would be more pronounced and the modified PB derived depth dose would deviate substantially from the open PB derived depth dose.

It was further found that the FDD deviation relative to that as calculated with the open PB increases as a function of compensator electron density. If the product of material density and Z/A (the mass electron density) is taken, the following electron densities (/cm^3) are obtained in units of N_A: wax

(0.67), aluminum (1.30), brass (3.87), copper (4.07), and lead (4.50). Since Compton interactions dominate at the studied PB energies, the electron density would play a significant role in the number of photon interactions that would take place per unit absorber thickness.

The match of the slope profiles in Figs. 3(b) and 3(d) at larger depths is not very accurate for wax, but yields reasonably accurate depth-dose data despite using smoothed slope data. These data were extracted by fitting Eqs. (3) and (4) to the $\Delta P_t^{(n)}/\Delta t$ data. The calculated FDD using the modified open PB corresponds to the FDD calculated using the actual filtered PB data. This indicates that the smoothing step does not alter the FDD data. The variance on the slope data originates from the set of MC simulations to obtain PB dose distributions, each having variance on the dose data in the PB dose distribution grid.

As a cautious generalization, it seems that the dose profile modeling scheme should also be applicable for other compensator materials over the energies studied, since the depth-dose curves for extreme compensator materials such as wax and lead could be modeled successfully.

E. Dose calculations under compensators using modified PBs

In Secs. III A and III B it was shown how the dose profiles for an open PB can be adjusted over depth to take compensator effects like beam filtering and scatter into account. In order to use the empirical formalism developed in the first part of the study in compensator dose calculations, the following steps would be performed for the case of a beam with uniform energy fluence:

(a) Determine the depth (z) of the plane at which the dose should be modulated on the open PB.
(b) Then, use the open PB dose profile at depth (z) as the basis for dose calculations.
(c) Calculate the value for $\alpha(r,z)$ from Eq. (3) and $\beta(r,z)$ from Eq. (4).
(d) If the PB traverses a compensator of thickness, t, then alter its dose profile using Eq. (5) with the correct values for $\alpha(r,z)$ and $\beta(r,z)$ at depth, z, as found in (c).
(e) Scale this PB dose profile at depth, z, with the effective attenuation coefficient as indicated in Eq. (7).
(f) Calculate the dose distribution in the plane of interest located at depth, z, for the modified PB at the relevant entrance site.
(g) Repeat this whole process (d)–(f) for all entrance positions of the PBs covering the field area, using the corresponding compensator thickness, t, for each entrance position.

The modified PB at depth z is calculated from

$$P_{t,\mathrm{med}}(r,z) = \{P_0(r,z) + [a_1 \exp(-a_2 r^2) + b_1(r-b_2) \times \exp(-b_3 r)]t\}\exp[-u_{\mathrm{eff}}(z)t], \quad (8)$$

where $P_0(r,z)$ is modeled with Eq. (1). Equation (8) can be modulated by taking the relative photon fluence at the location in the beam into account.

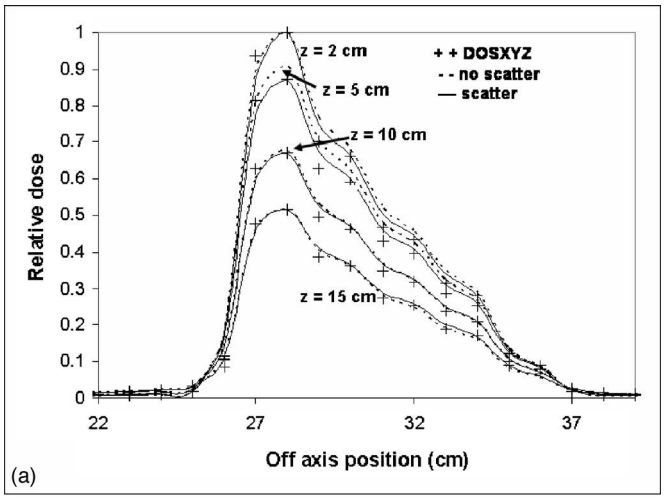

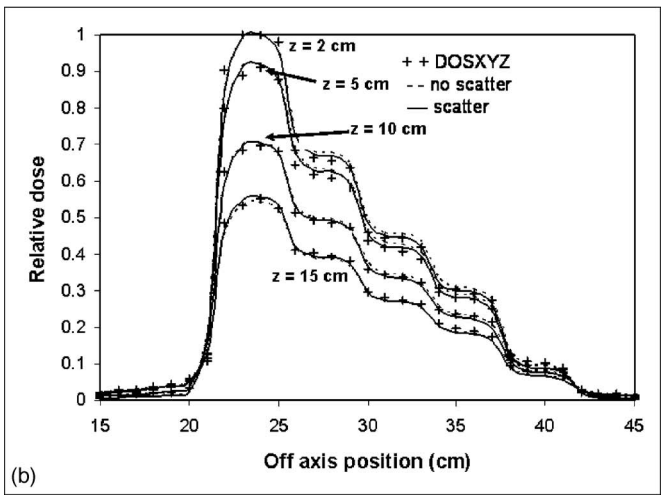

FIG. 6. Relative dose profiles for (a) $10\times10\ \mathrm{cm}^2$ field and (b) $20\times20\ \mathrm{cm}^2$ field calculated under a copper step wedge for a 6 MV beam energy. The DOSXYZ profiles are used as the benchmark data and have a variance of 1 percent. The PB dose profiles have been calculated without scatter (broken lines) and with scatter (solid lines).

In Figs. 5(a) and 5(b) it was shown how the inclusion of compensator-induced effects such as beam filtering and photon scatter can alter the FDD for circular fields. If only the open PB was used and its intensity was scaled with an effective attenuation coefficient, the dose could be tailored in one plane only and not throughout the volume.

Calculations for a step wedge copper compensator material for 6 MV and a field size of $10-10\ \mathrm{cm}^2$ and $20\times20\ \mathrm{cm}^2$ are shown in Figs. 6(a) and 6(b), respectively. Dose profiles were compared at depths of 2, 5, 10, and 15 cm. The DOSXYZnrc Monte Carlo data were used as the reference data since they included all scatter effects from the compensating medium. The compensator to water phantom surface distance was set at 33 cm. The PB calculations were performed for the case where scatter was switched off and a effective attenuation coefficient (μ_{eff}=0.403/cm) was used to best fit the dose profile at 10 cm depth. The effective

attenuation coefficient was determined from a least-square error procedure to best fit the dose profile at the depth of interest. In the other case the scatter effects were included and another effective attenuation coefficient (μ_{eff} =0.417/cm) was used to best fit the dose profile at 10 cm depth. Note that the effective attenuation value in the case without scatter is about 3.5 percent lower to compensate for scatter. At the reference depth of 10 cm the two methods can be made to correspond to a high degree of accuracy when compared with the DOSXYZnrc data. However, at 2 cm depth the scatter-included data more closely follow the DOSXYZnrc data compared to the no-scatter data as observed for both field sizes. The exclusion of scatter can lead to dose errors of up to 4 percent. For materials such as lead this discrepancy could be as high as 7 to 8 percent. For larger fields the effect of in-phantom scatter reduces the differences in the dose profiles where scatter is modeled explicitly or where an effective attenuation coefficient is used.

If an effective attenuation coefficient (EAC) for a certain field was measured, using it with compensators for the same field does not yield the best fit to, say, benchmark data like those obtained with MC methods. The EAC should in this case compensate for missing scatter modeling if the PB model is used without scatter adjustments. In this case we would expect an EAC value representative of a larger field. To obtain the best EAC value it is best to calculate dose profiles, compare against benchmark data, and adjust the coefficient until the least-square error is minimized.

For the case where the PB is adjusted to include scatter and beam hardening effects, the EAC must be obtained using a least-square method to best fit the data. The difference here is that the same EAC value can be used over a wide range of field sides and does not change as a function of field size as in the above-mentioned case. This EAC represents that for a narrow beam or finite-sized PB.

The method of using an EAC without changing the PB dose profiles can be used to replicate benchmarked dose profiles at any desired depth. But, the accuracy will hold at this depth only. In the proposed method much better accuracy is obtained at all the other depths. A prime concern is the use of dose calculation models where compensators are used in IMRT. We think that it would be more advantageous to be able to calculate the dose under a compensator accurately over a range of depths, rather than just one plane, since one is interested in optimizing the dose distribution in a volume.

The studies have been conducted for PB dose profile modeling at a SSD of 100 cm. If the SSD is increased, then compensator scattered photons would deposit energy at larger radial locations from the CAX. Thus, at a certain off-axis location an increase in the relative dose is foreseen that would influence the dose profile fitting parameters, since, relative to the open PB ($\Delta P^{(n)}_{t,\text{med}}/\Delta t$) would increase.

IV. CONCLUSION

In this study it was found that the relative dose for a set of normalized PBs, after traversing various thicknesses of wax, aluminum, brass, copper, and lead, was linear in the material thickness as expressed by Eq. (4). The slopes of the lines of relative dose vs absorber thickness were defined as $\Delta P_{t,\text{med}}/\Delta t$ and could be decomposed into two parts, of which $\alpha(r,z)$ is a Gaussian and is fitted to the PB beyond its transition radius that is a function of energy and compensator material. The fitting functions could successfully reproduce the normalized depth-dose data when compared to depth dose curves produced by the actual filtered PBs for 5 cm of filtered material (wax=12 cm) for 10 and 20 cm circle fields. Thus, a PB parametrization scheme such as the one developed in this study can be used to parametrize dose profiles at each depth for an open PB to include the effects of compensator materials. This approach can then be applied to compensators where a superposition method can be used to calculate the dose in water at a certain reference depth. It was further found that the method developed here leads to more accurate dose profile modeling near the phantom surface compared to methods that include compensator scatter through an effective attenuation coefficient where the dose profiles were matched at 10 cm depth.

[a]Current address: Medical Physics Department, Faculty of Medicine, University of the Free State, P.O. Box 339, Bloemfontein, 9300 South Africa. Electronic mail: duplesf@fshealth.gov.za

[1]S. V. Spirou and C. S. Chui, "Generation of arbitrary intensity-profiles by dynamic jaws or multileaf collimators," Med. Phys. **21**, 1031–1041 (1994).
[2]S. Webb, "Intensity-modulated radiation therapy using only jaws and a mask," Phys. Med. Biol. **47**, 257–275 (2002).
[3]S. X. Chang, T. J. Cullip, K. M. Deschesne, E. P. Miller, and J. G. Rosenman, "Compensators: An alternative IMRT delivery technique," J. Appl. Clin. Med. Phys. **5**, 15–36 (2004).
[4]K. Yoda and Y. Aoki, "A multiportal compensator system for IMRT delivery," Med. Phys. **30**, 880–886 (2003).
[5]K. Nakagawa, N. Fukuhara, and H. Kawakami, "A packed building-block compensator (TETRIS-RT) and feasibility for IMRT delivery," Med. Phys. **32**, 2231–2235 (2005).
[6]T. Xu, P. M. Shikhaliev, M. Al-Ghazi, and S. Molloi, "Reshapable physical modulator for intensity modulation radiation therapy," Med. Phys. **29**, 2222–2229 (2002).
[7]J. H. Kung, G. T. Y. Chen, and F. K. Kuchnir, "A monitor unit verification calculation in intensity modulated radiotherapy as a dosimetry quality assurance," Med. Phys. **27**, 2226–2230 (2000).
[8]M. R. Arnfield, J. V. Siebers, J. O. Kim, Q. Wu, P. J. Keall, and R. Mohan, "A method for determining multileaf collimator transmission and scatter for dynamic intensity modulated radiotherapy," Med. Phys. **27**, 2231–2241 (2000).
[9]J. D. Azcona, R. A. C. Siochi, and I. Azinovic, "Quality assurance in IMRT: Importance of the transmission through the jaws for accurate calculation of absolute doses and relative distributions," Med. Phys. **29**, 269–274 (2002).
[10]L. Wang, C.-S. Chui, and M. Lovelock, "A patient-specific Monte Carlo dose-calculation method for photon beams," Med. Phys. **25**, 867–878 (1998).
[11]J. S. Li, T. Pawlicki, J. Deng, S. B. Jiang, E. Mok, and C.-M. Ma, "Validation of a Monte Carlo dose calculation tool for radiotherapy treatment planning," Phys. Med. Biol. **45**, 2969–2985 (2000).
[12]O. Z. Ostiapak, Y. Zhu, and J. Van Dyk, "Refinements of the finite-size pencil beam model of three-dimensional photon dose calculation," Med. Phys. **24**, 743–750 (1997).
[13]A. Boyer, L. Xing, C.-M. Ma, B. Curran, R. Hill, A. Kania, and A. Bleier, "Theoretical considerations of monitor unit calculations for intensity modulated beam treatment planning," Med. Phys. **26**, 187–195 (1999).
[14]B. Zackrisson, M. Arevärn, and M. Karlsson, "Optimized MLC-beam arrangements for tangential breast irradiation," Radiother. Oncol. **54**, 209–212 (2000).
[15]L. Weber and F. Laursen, "Dosimetric verification of modulated photon

fields by means of compensators for a kernel model," Radiother. Oncol. **62**, 87–93 (2002).
[16]J. V. Siebers, M. Lauterbach, S. Tong, Q. Wu and R. Mohan, "Reducing dose calculation time for accurate iterative IMRT planning," Med. Phys. **29**, 231–237 (2002).
[17]P. S. Basran, W. Ancbacher, G. C. Field, and B. R. Murray, "Evaluation of optimized compensators on a 3D planning system," Med. Phys. **25**, 1837–1844 (1998).
[18]W. Laub, M. Alber, M. Birkner, and F. Nüsslin, "Monte Carlo dose computation for IMRT optimization," Phys. Med. Biol. **45**, 1741–1754 (2000).
[19]A. Ahnesjö, L. Weber, and P. Nilsson, "Modeling transmission and scatter for photon beam attenuators," Med. Phys. **22**, 1711–1721 (1995).
[20]A. Ahnesjö, "Analytical modeling of photon scatter from flattening filters in photon therapy beams," Med. Phys. **21**, 1227–1235 (1994).
[21]A. Ahnesjö, "Collimator scatter in photon therapy beams," Med. Phys. **22**, 267–278 (1994).
[22]E. L. Chaney and T. J. Cullip, "A Monte Carlo study of accelerator head scatter," Med. Phys. **21**, 1383–1390 (1994).
[23]A. Ahnesjö, M. Saxner, and A. Trepp, "A pencil beam model for photon dose calculation," Med. Phys. **19**, 263–273 (1991).
[24]M. K. Islam and J. Van Dyk, "Effects of scatter generated by beam-modifying absorbers in megavoltage photon beams," Med. Phys. **22**, 2075–2081 (1995).
[25]A. Ahnesjö and M. M. Aspradakis, "Dose calculations for external photon beams in radiotherapy," Phys. Med. Biol. **44**, R99–R155 (1999).
[26]P.-H. Huang, L. M. Chin, and B. E. Bjärngard, "Scattered photons produced by beam-modifying filters," Med. Phys. **13**, 57–63 (1986).
[27]E. Papiez and G. Froeze, "The calculation of transmission through a photon beam attenuator using sector integration," Med. Phys. **17**, 281–286 (1990).
[28]M. E. Castelanos and J. C. Rosenwald, "Evaluation of the scatter field for high-energy photon beam attenuators," Phys. Med. Biol. **43**, 277–290 (1998).
[29]L. Weber and F. Laursen, "Dosimetric verification of modulated photon fields by means of compensators for a kernel model," Radiother. Oncol. **62**, 87–93 (2001).
[30]D. W. O. Rogers, I. Kawrakow, J. P. Seuntjens, B. R. B. Walters, and Mainegra-Hing "NRC User Codes for EGSnrc," NRCC Report PIRS-702 (revB), 50–56 (2005).
[31]I. Kawrakow, "Accurate condensed history simulation of electron transport. I. EGSnrc, the new EGS4 version," Med. Phys. **27**, 485–498 (2000).
[32]F. C. P. du Plessis and C. A. Willemse, "Monte Carlo calculation of effective attenuation coefficients for various compensator materials," Med. Phys. **30**, 2537–2544 (2003).
[33]W. R. Nelson, H. Hirayama, and D. W. O. Rogers, "The EGS4 Code System SLAC-Report-265," Stanford Linear Accelerator Center (1985).
[34]D. W. O. Rogers, B. A. Faddegon, G. X. Ding, C.-M. Ma, J. We, and T. R. Mackie, "BEAM: A Monte Carlo code to simulate radiotherapy treatment units," Med. Phys. **22**, 503–525 (1995).
[35]C.-M. Ma and D. W. O. Rogers, "BEAMDP Users Manual," National Research Council of Canada. Report PIRS-0509B (NRC, Ottawa), (1995).
[36]P. Storchi and E. Woudstra, "Calculation of the absorbed dose distribution due to irregularly shaped photon beams using pencil beam kernels derived from basic beam data," Phys. Med. Biol. **41**, 637–656 (1996).
[37]L. Wang and S. L. Jacques, "Optimized radial and angular positions in Monte Carlo modeling," Med. Phys. **21**, 1081–1083 (1994).
[38]B. Walters, I. Kawrakow, and D. W. O. Rogers, "DOSXYZnrc Users Manual," NRCC Report PIRS-794 (revB), 1–97 (2005).
[39]Y. Mejaddem, S. Hyödynmaa, R. Svenson, and A. Brahme, "Photon scatter kernels for intensity modulating radiation therapy filters," Phys. Med. Biol. **46**, 3215–3228 (2001).